MFN= 007394
01 SID/SCD
02 6019
03 INPE-6019-PRE/2134
04 MER
05 S
06 as
10 Pereira, Claudio Solano
10 Mascarenhas Jr., Affonso da S
12 Numerical simulation of a response of an oceanic front to an atmospheric frontal passage
14 16081-16093
30 Journal of Geophysical Research
31 99
32 C8
40 En
41 En
42 <E>
58 CPTC
61 <P>
64 Aug. <1994>
68 PRE
76 CIENCIAS METEOROLOGICAS
83 The influence of middle cyclones and their associated clod fronts on open-ocean fronts is studied with an embedded mixed layer ocean circulation model similar to that of Adamec et al. (1981). Finite differences with horizontal resolution of 5 km in a staggered grid are used to solve the model equations within a domain of tatal meridional extension of 300 km and 500 m depth. three numrical experiments were performed to investigate the response of an oceanic front, similar to the South Atlantic subtropical convergence zone, to an atmospheric frontal passage. Under the effect of the cold air outbreak the thermal and dynamic structures of the upper layer are substantially modifield with a higher singking/cooling rate of the mixed layer. The sinking/cooling rate depends strongly on the magnitude of the thermal gradient at the top of the thermocline and on the mixed layer depth. Due to the differences in sinking/cooling rates, a single storm can move the oceanic front up to 20 km from its initial the position. For low-intensity winds, a change in the wind direction does not affect the thermal structure of the upper layer ocean, even inthe frontal region. The mixed layer oscillations are entirely a function of the daily scale of the solar heating. For a sudden change in the wind direction, the response of the current velocity field in the mixed layer is almost instantaneous.
87 ESTUDO DO TEMPO$SIMULACAO NUMERICA
90 b
91 FDB-19961017
92 FDB-MLR

JOURNAL OF GEOPHYSICAL RESEARCH, VOL. 99, NO. C8, PAGES 16,081–16,094, AUGUST 15, 1994

Numerical simulation of a response of an oceanic front to an atmospheric frontal passage

Claudio Solano Pereira[1]

Centro de Previsao de Tempo e Estudos Climaticos, Instituto de Pesquisas Espaciais
São José dos Campos, Brazil

Affonso da S. Mascarenhas Jr.

Instituto de Investigaciones Oceanológicas, Universidad Autónoma de Baja California, Ensenada, Mexico

Abstract. The influence of middle-latitude cyclones and their associated cold fronts on open-ocean fronts is studied with an embedded mixed layer ocean circulation model similar to that of Adamec et al. (1981). Finite differences with horizontal resolution of 5 km in a staggered grid are used to solve the model equations within a domain of total meridional extension of 300 km and 500 m depth. Three numerical experiments were performed to investigate the response of an oceanic front, similar to the South Atlantic subtropical convergence zone, to an atmospheric frontal passage. Under the effect of the cold air outbreak the thermal and dynamic structures of the upper layers are substantially modified with a higher sinking/cooling rate of the mixed layer. The sinking/cooling rate depends strongly on the magnitude of the thermal gradient at the top of the thermocline and on the mixed layer depth. Due to the differences in sinking/cooling rates, a single storm can move the oceanic front up to 20 km from its initial position. For low-intensity winds, a change in the wind direction does not affect the thermal structure of the upper layer ocean, even in the frontal region. The mixed layer oscillations are entirely a function of the daily scale of the solar heating. For a sudden change in the wind direction, the response of the current velocity field in the mixed layer is almost instantaneous.

1. Introduction

The main impact of the ocean on the atmosphere occurs through the magnitude and distribution of the sea surface temperature. In addition, the ocean mixed layer is constantly subjected to atmospheric effects in the ocean-atmosphere interface in the form of momentum, latent and sensible heat, and radiation transfers. These energy exchanges constantly modify the thermal and dynamical structures of the upper ocean, which can also be affected by mesoscale and large-scale phenomena which occur in the "subsurface" ocean [*Stevenson*, 1980].

In mid-latitudes the dominant atmospheric timescales are longer than $1/f$, with length scales between 500–2000 km [*Fissel*, 1976]. Even though the large steady state low-pressure centers or steady state zonal jets can cause strong wind stresses on the ocean surface, these synoptic perturbations will not excite inertial oscillations in the oceanic mixed layer [*D'Asaro*, 1985b]. On the other hand, atmospheric events associated with cold front passages or small secondary lows are the major contributors providing turbulent kinetic energy for mixing the upper layer of the ocean [*Elsberry and Haney*, 1978; *Haney et al.*, 1981]. These events are very effective in generating mesoscale variations (30–2000 km) in the ocean [*Orlanski and Polinsky*, 1983] and in exciting inertial oscillations [*D'Asaro*, 1985a, b].

In a general way, South American atmospheric cold fronts are persistent over the year, moving swiftly from the southern South American coast toward the northeast [*Girardi*, 1972]. These cold fronts display strong wind bands that are aligned mostly perpendicular to the coast and move northeastward until they dissipate at low latitudes [*Kousky*, 1978].

A dominant oceanographic feature characteristic of the subtropical western South Atlantic off the Brazilian and Uruguayan coast is a sharp discontinuity in surface temperature and salinity as result of the Brazil-Malvinas current confluence [*Tseng*, 1976; *Reid et al.*, 1977; *Legeckis and Gordon*, 1982; *Godoi*, 1983; *Roden*, 1986; *Ikeda et al.*, 1986]. Satellite and oceanographic observations have shown that the mean position of the convergence is around 40°S. Most of the studies concerning the convergence displacements are aimed toward a seasonal behavior, even though there exists evidence showing significant displacements at much shorter timescales [*Legeckis and Gordon*, 1982].

This work was motivated by the strong relation between small-scale meteorological phenomena and the thermal-hydrodynamical structure of the upper ocean. Numerical experiments were performed in order to evaluate the effects of atmosphere-ocean transfer processes over the thermal and dynamical structure of an ocean front as the result of an atmospheric frontal passage. The model used is that proposed by *Adamec et al.* [1981], where the effects of advection, diffusion, and mixing in the upper ocean are considered. This work is distinct from that of *Adamec and*

[1]On sabbatical at Laboratoire D'Océanographie Dynamique et de Climatologie, Paris.

Paper number 94JC00969.
0148-0227/94/94JC-00969$05.00

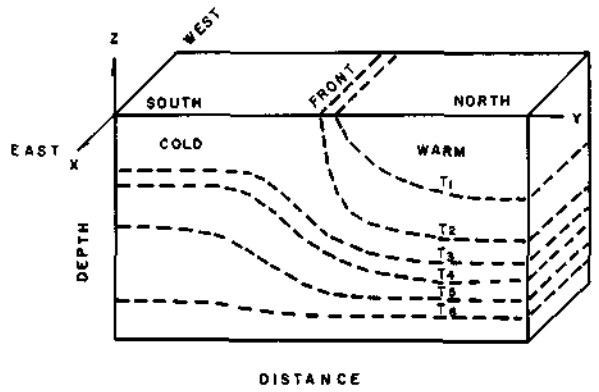

Figure 1. Schematic representation of the coordinate system: x (zonal), y (meridional), z (vertical). The y-z plane is perpendicular to an ocean front caused by the convergence of two ocean currents (the colder is on the south side).

Garwood [1985] in the sense that the numerical approach is different, and the momentum and buoyancy fluxes try to simulate mainly one of the phases occurring during an atmospheric cold front passage, the cold air outbreak over the ocean.

In section 2 the ocean circulation model, in which a mixed layer model is embedded, is discussed with the respective hypotheses, boundary conditions, and parametrizations. In section 3 the numerical analysis of the problem is treated. The specific initial conditions and the results of the numerical experiments are discussed in section 4. Finally, in section 5 the model deficiencies which limit its applications and the results are discussed.

2. Circulation Model Coupled to a Mixed Layer Model

2.1. Multilevel Circulation Model: Hypothesis and Equations

Consider a Boussinesq fluid, on an f plane where the molecular viscosity and conductivity and double-diffusion processes are neglected. Generally speaking, the salinity plays a small role in the mixed layer dynamics at mid-latitudes [*Frankignoul*, 1985], so here it will be neglected. This means that the conservation of buoyancy is reduced to the conservation of heat only; nevertheless, buoyancy will be maintained in the equations. The oceanic front will be considered infinite in the zonal direction, implying that the ocean response is independent of x (Figure 1). The model is two-dimensional considering a vertical plane, y-z, transversal to the front, thus allowing a zonal velocity component. Under those assumptions the governing equations in flux form are

Equation of state

$$b = \alpha(T - T_0) \tag{1}$$

Conservation of thermodynamical energy

$$\frac{\partial b}{\partial t} = -\frac{\partial}{\partial y}(vb) - \frac{\partial}{\partial z}(wb) + \frac{\partial}{\partial y}(-\overline{v'b'}) + \frac{\partial}{\partial z}(-\overline{w'b'}) \tag{2}$$

Conservation of mass

$$\frac{\partial v}{\partial y} + \frac{\partial w}{\partial z} = 0 \tag{3}$$

Conservation of horizontal momentum

$$\frac{\partial u}{\partial t} = -\frac{\partial}{\partial y}(uv) - \frac{\partial}{\partial z}(uw) + fv + \frac{\partial}{\partial y}\overline{(-v'u')} + \frac{\partial}{\partial z}\overline{(-w'u')} \tag{4}$$

$$\frac{\partial v}{\partial t} = -\frac{\partial}{\partial y}(vv) - \frac{\partial}{\partial z}(vw) - fu - \frac{\partial p}{\partial y} + \frac{\partial}{\partial y}(-\overline{v'v'}) + \frac{\partial}{\partial z}(-\overline{w'v'}) \tag{5}$$

Hydrostatic relation

$$\frac{\partial p}{\partial z} = b \tag{6}$$

where $p = gz + p_r/\rho_0$ is the dynamic pressure, p_r the reference state pressure, and ρ_0 a reference density. The set of equations (1) to (6) are applied to an ocean region 300 km long along the meridional coordinate y and 500 m deep.

2.1.1. Boundary and initial conditions. The problem posed is an initial boundary value problem, where the equations will be numerically integrated. There are four prognostic equations in the unknowns u, v, w, and b, for which initial conditions will characterize the ocean front in the numerical experiments. The rigid lid condition is imposed on the sea surface [e.g., *Orlanski and Polinsky*, 1983]:

$$z = 0, \qquad w = 0 \tag{7}$$

This is not a strong restriction, since we are interested in movements with frequencies near the inertial [*Veronis*, 1956]. In addition, the removal of the external gravity wave allows us the use of larger time steps in the numerical integration. At the surface the wind stress and the buoyancy fluxes are also prescribed:

$$-\overline{(u'w')} = \frac{\tau_0^x}{\rho_0} \tag{8}$$

$$-\overline{(v'w')} = \frac{\tau_0^y}{\rho_0} \tag{9}$$

$$-\overline{(b'w')} = B_0 \tag{10}$$

The boundary conditions at the bottom, $z = -H$, are vanishing vertical velocity and no turbulent fluxes of momentum and buoyancy:

At $z = -H$,

$$w = 0$$

$$\overline{(u'w')} = \overline{(v'w')} = \overline{(b'w')} = 0 \tag{11}$$

At the lateral boundaries ($y = 0$, $y = L$), the radiation boundary condition was used [*Camerlengo and O'Brien*, 1980].

2.1.2. Parametrization of the turbulent fluxes. In order to represent the lateral turbulent diffusion as well as the vertical profiles in the layer below the wind influence, they are expressed as the gradient of the transported quantity multiplied by an appropriate eddy diffusion coefficient [*Rooth and Ostlund*, 1972].

In the horizontal

$$\overline{(v'u')} = -A_M \frac{\partial u}{\partial y} \qquad \overline{(v'v')} = -A_M \frac{\partial v}{\partial y}$$

$$\overline{(v'b')} = -A_B \frac{\partial b}{\partial y} \tag{12}$$

In the vertical, below the mixed layer

$$\overline{(u'w')} = -K_M \frac{\partial u}{\partial z} \qquad \overline{(v'w')} = -K_M \frac{\partial v}{\partial z}$$

$$\overline{(b'w')} = -K_B \frac{\partial b}{\partial z} \tag{13}$$

where A_M and A_B are the horizontal turbulent coefficients of momentum and buoyancy, and K_M and K_B are the respective vertical coefficients.

Within the mixed layer, however, these parametrizations are not ideal, due to the variability of the turbulent coefficients [*Welander*, 1957; *Veronis*, 1975; *Pollard*, 1977; *Ramming and Kowalik*, 1980]. In order to parametrize the momentum and buoyancy turbulent fluxes within the mixed layer, the assumption that those fluxes are linear functions of z is made. At the mixed layer top, the fluxes are those specified by (8), (9) and (10). At the mixed layer bottom, $z = -h$, the turbulent fluxes are specified by (15), (16), and (17), in section 2.2.

In this way the parametrizations utilized in this work use the mixed layer depth h [*Garwood*, 1977]. A prognostic equation for h is obtained through the integration of the continuity equation (3) in the mixed layer and the boundary condition at $z = 0$, equation (7):

$$\frac{\partial h}{\partial t} + \frac{\partial}{\partial y} h\langle v\rangle = \frac{dh}{dt} + w(-h) = w_e \tag{14}$$

where angle brackets denote a vertical mean within the mixed layer.

The parametrization of w_e will be given in the next section (2.2) within the development of the mixed layer model. The important fact to be pointed out is that the turbulent flux parametrizations within the mixed layer are done as a function of h, such that the dynamic nature of the time and space variations of the turbulent coefficients is accounted for by the variations in h. This allows a relationship between cause and effect in the parametrizations, justifying the need for connecting a mixed layer model to a multilayer circulation model.

The equations (2) to (6) and (14), with the boundary conditions given by (7) to (11) and the turbulent quantities parametrized, form a closed set of equations in six variables u, v, w, p, b, and h.

2.2. Mixed Layer Model: Hypothesis and Equations

Here, as in the work by *Adamec et al.* [1981], there is a balance between the buoyancy flux in the entrainment layer and the convergence flux of turbulent kinetic energy in the mixed layer model. This convergence term is assumed to be a function of the turbulent kinetic energy and of the distance over which this energy must be transported:

$$\overline{(b'w')}(-h) = -\frac{\overline{\langle w'w'\rangle}^{1/2}\langle \bar{e}_k\rangle}{h} \tag{15a}$$

where $\langle \bar{e}_k\rangle$ is the mean value of the total turbulent kinetic energy and $\overline{\langle w'w'\rangle}^{1/2}$ is twice the vertical component mean value of the turbulent kinetic energy in the mixed layer.

The prognostic equations for these turbulent variables are

$$\frac{\partial}{\partial t}\left[h\frac{\overline{\langle u'^2 + v'^2\rangle}}{2}\right] = m_3 u_*^3 - \frac{h}{2R_i^*}\overline{(w'b')}_{-h} - (\overline{\langle e_k\rangle} - 3\overline{\langle w'w'\rangle})\overline{\langle e_k\rangle}^{1/2} - \tfrac{2}{3}(\overline{\langle e_k\rangle}^{1/2} - fh)\overline{\langle e_k\rangle} \tag{15b}$$

$$\frac{\partial}{\partial t}\left[h\frac{\overline{\langle w'w'\rangle}}{2}\right] = \tfrac{1}{2}h[\overline{(w'b')}_{-h} - \overline{(w'b')}_{z=0}] + (\overline{\langle e_k\rangle} - 3\overline{\langle w'w'\rangle})\overline{\langle e_k\rangle}^{1/2} - \tfrac{1}{3}(\overline{\langle e_k\rangle}^{1/2} - fh)\overline{\langle e_k\rangle} \tag{15c}$$

where m_3 is a constant to be tuned during the numerical experiment, u_* is the mixed layer friction velocity, and R_i^* is the mixed layer overall Richardson number.

Once the values of u_*, $\overline{(w'b')}_{z=0}$, h, and R_i^* are specified and the quasi-stationary state for the turbulent kinetic energy supply is assumed, i.e.,

$$\frac{\partial}{\partial t}(h\overline{\langle e_k\rangle}) \approx 0 \qquad \frac{\partial}{\partial t}(h\overline{\langle w'w'\rangle}) \approx 0 \tag{15d}$$

the buoyancy flux due to entrainment is determined by (15a)–(15d).

Once the buoyancy flux is known at the base of the mixed layer (equation (15a)), we obtain the entrainment-associated momentum fluxes at the base of the mixed layer, $\overline{u'w'}(-h)$ and $\overline{v'w'}(-h)$, by the parametrizations

$$-\overline{u'w'}(-h) = -\frac{\overline{b'w'}(-h)}{\Delta b}\Delta u = w_e \Delta u \tag{16}$$

$$-\overline{v'w'}(-h) = -\frac{\overline{b'w'}(-h)}{\Delta b}\Delta v = w_e \Delta v \tag{17}$$

where the entrainment velocity is given by

$$w_e = -\frac{\overline{b'w'}(-h)}{\Delta b} \tag{18}$$

and where Δb, Δu, and Δv are the buoyancy and horizontal velocity jumps in entrainment layer. A detailed derivation of the prognostic equations for the turbulent variables is given by *Garwood* [1977].

The mixed layer retraction occurs when the vertical component of the turbulent kinetic energy is not sufficient to transport momentum and heat to the previously established mixed layer base. In this way, the criterion adopted to know if there is retraction is to check the value of the vertical component of the turbulent kinetic energy, which in this case must be close to zero; the limiting value established was $\overline{\langle w'w'\rangle}^{1/2} \leq 10^{-8}$. The implication of this is that (15a) is no

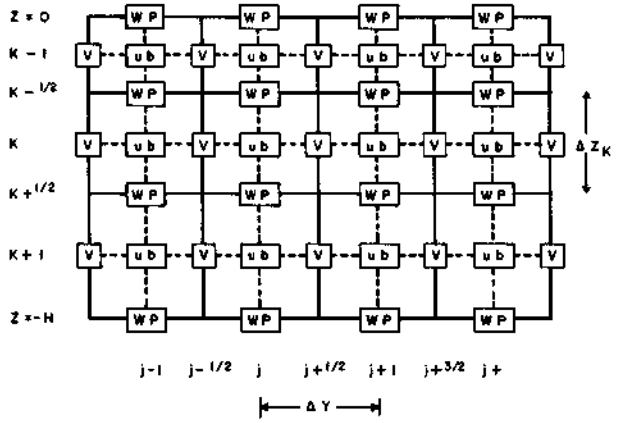

Figure 2. Distribution of the variables on the grid in the y-z plane.

longer used to compute h, and (15b) and (15c) in the steady state are reduced to

$$m_3 u_*^3 - \langle\overline{e_k}\rangle^{3/2} - \tfrac{2}{3}(\langle\overline{e_k}\rangle^{1/2} - fh)\langle\overline{e_k}\rangle = 0 \qquad (18a)$$

$$-\frac{h}{2}\langle\overline{w'b'}\rangle_{z=0} + \langle\overline{e_k}\rangle^{3/2} - \tfrac{1}{3}(\langle\overline{e_k}\rangle^{1/2} - fh)\langle\overline{e_k}\rangle = 0 \qquad (18b)$$

One of the principal parameters in the mixed layer evolution is the dynamical instability at its base. The overall Richardson number, $R_i^* = h\Delta b/(\Delta u^2 + \Delta v^2)$, governs the beginning of the instability by shear, for values below 0.25 [*Turner*, 1973; *Pollard et al.*, 1973; *Kullenberg*, 1976].

In order to ensure the stability of the density and momentum profiles in the column below the mixed layer, a convective adjustment is imposed based on the local value of R_i. *Adamec et al.* [1981] give a very good explanation of the coupling process between the multilayer model and the mixed layer model as well as the convective adjustment.

3. Numerical Model

The alternating grid and the spacewise finite differentiation numerical schemes used in the model are different from those used by *Adamec et al.* [1981]. The grid is shown in Figure 2. In the horizontal the C scheme of Arakawa [*Mesinger and Arakawa*, 1976] is used, and in the vertical, the C′ scheme of *Tokioka* [1978].

The finite difference scheme in space is of second order, and the chosen grid allows energy conservation [*Elsberry et al.*, 1984]. In addition, it prevents the occurrence of computational modes in space [*Haney*, 1974].

The grid configuration in the y-z plane shown in Figure 2 has the following geometrical characteristics: L, horizontal length of the grid, equals 300 km; H, vertical length of the grid, equals 500 m; Δy, horizontal grid point interval, equals 5 km; and k, number of levels, equals 8.

The vertical structure is represented by eight discrete layers, which are enough to resolve the vertical structure in our case. The vertical resolution varies exponentially from 10 m at the surface to 175 m at a depth of 500 m.

The time differentiation is made through a "leapfrog" iteration with a Matsuno scheme [*Mesinger and Arakawa*, 1976] every 15 time steps. The advective and Coriolis terms are explicit, and the diffusive terms lag by one time step. The pressure gradient term is handled using a Brown and Campana scheme [*Haltiner and Williams*, 1980]. With these schemes and the radiational boundary condition it is possible to use a 30-min time step for the numerical integration.

In a general way this model treats the dynamic and mixing processes in two mutually interconnected steps: (1) the dynamic one, within which the advective and diffusive processes are included; and (2) the mixing one, where the changes due to entrainment feed back to the dynamical part of the model. During those two phases, a special treatment is given for the level that contains the bottom of the mixed layer [*Adamec et al.*, 1981].

4. Numerical Experiments: Results

4.1. Initial Conditions for the Numerical Integration

The numerical experiments should exhibit the dependence of the upper ocean response to the parameters characterizing the atmospheric cold front. The atmospheric forcing during the experiment is specified a priori and is modeled to represent the cold air outbreak during the cold front passage, characterized by the wind intensification and upward heat fluxes from the ocean to the atmosphere.

The initial field of temperature and mixed layer depth are smoothed versions of *Legekis and Gordon*'s [1982] data. The vertical temperature field is shown in Figure 3, where a strong horizontal temperature gradient indicates the position of the frontal zone, and the slopes of the isotherms suggest the presence of vertical motions. The initial distribution of the mixed layer depth is shown in Figure 4, where the frontal zone is identified by a sudden variation in the mixed layer depth.

Four quantities describe the response of the oceanic front: (1) the mixed layer temperature, (2) the mixed layer depth, (3) the horizontal velocity in the mixed layer, and (4) the vertical velocity. These quantities are monitored during the 120 hours of integration of the model.

During the first numerical experiment (EXP.I), the wind stress, $\tau(t)$, and the surface buoyancy flux, $B_0(t)$, are uniformly distributed in space, simulating a storm generated and extinguished over the same region. In the second experiment (EXP.II), the surface buoyancy fluxes are withdrawn, leaving only the wind stress as atmospheric forcing. Finally, in the third experiment (EXP.III) the initial conditions and the surface buoyancy fluxes are the same as

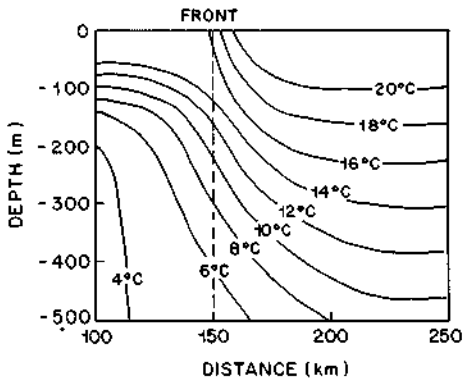

Figure 3. Initial cross-front thermal structure of the upper 500 m. The numbers indicate the temperature of the isotherms (degrees Celsius).

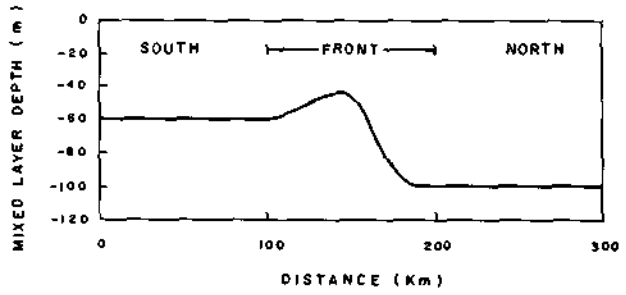

Figure 4. The initial distribution of the cross-front mixed layer depth.

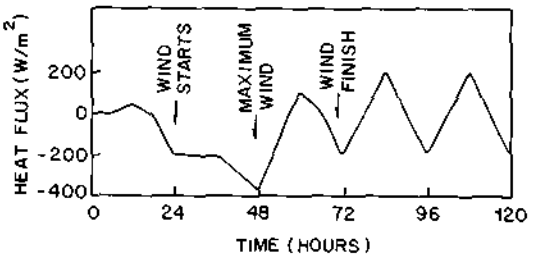

Figure 6. Sea surface net heat flux. Positive values are from the atmosphere to the ocean.

(EXP.I), and the rotation of the wind stress is considered but its magnitude is maintained constant.

4.2. Results and Discussions of EXP.I

The wind stress is a function of the time and is calculated as

$$\tau = \rho_a C_D |\mathbf{u}_a| \mathbf{u}_a \tag{19}$$

where ρ_a is the air density and C_D a drag coefficient, depending on the wind velocity as [*Garratt*, 1977]:

$$C_D = 0.00075 + 6.7 \times 10^{-5} u_a \tag{20}$$

where $\mathbf{u}_a$ is the wind velocity in meters per second.

Since the storm conditions are brief and localized [*Dillon and Caldwell*, 1978] and the high-frequency fluctuations in the wind field have no significant effect on the momentum transfer at the air-sea interface [*Price*, 1981], a storm can be represented by the simple function shown in Figure 5 [*Marchuk et al.*, 1977] and expressed by

$$\begin{aligned} |\mathbf{u}_a(t)| &= 4 \quad \text{(m/s)} && t < 24 \text{ hours} \\ |\mathbf{u}_a(t)| &= 4 + 16(t - 24)/24 && 24 \le t < 48 \text{ hours} \\ |\mathbf{u}_a(t)| &= (20 - 16)(t - 48)/24 && 48 \le t < 72 \text{ hours} \\ |\mathbf{u}_a(t)| &= 4 \quad \text{(m/s)} && t \ge 72 \text{ hours} \end{aligned} \tag{21}$$

We are assuming a SW wind, which implies $\tau_x = \tau_y = |\tau| \cos 45°$. The functions $\mathbf{u}_a(t)$ and $|\tau(t)|$ are shown in Figure 5.

The atmospheric conditions during the first 24 hours are considered fair, with winds of 4 m/s, reaching a maximum of 20 m/s in the next 24 hours, during the storm peak. In the following 24 hours the wind velocity decays symmetrically until it returns to the 4 m/s value; then it remains constant until the end of the 120 hours of integration of the model.

The surface heat fluxes are extracted from real data, representing a typical storm passage over the ocean [*Nowlin and Parker*, 1974; *Sethuraman et al.*, 1986] and are displayed in Figure 6. The heat flux integrated along a 5-day period exhibits a net heat loss of 27.2×10^6 W/m^2. This heat loss is due mainly to the high latent heat exchange caused by the strong winds and by the presence of dry, cold air after the cold front passage.

Usually, as suggested by *Van Woert* [1982], the velocity component along a steady oceanic front is assumed to be in geostrophic equilibrium. Thus we assume here that in the initial instant, the u component is in geostrophic equilibrium, and the v component, transversal to the front, vanishes in all points of the grid. With the fields obtained in that way, a uniformization of the mixed layer variables is promoted, which leads, on the surface, to velocities smaller than those in geostrophic balance.

In order to characterize the horizontal ocean variability, we considered three regions: the region south of the ocean front (S), at 75 km from the coordinate origin; the frontal region (F), at 150 km from the origin; and the region north of the ocean front (N), at 225 km from the origin, (Figure 4). From now on, these regions will be referred to as S, F, and N.

The time evolution of the mixed layer temperature and depth for the regions S, F, and N is shown in Figures 7, 8 and 9. During the first 24 hours the mixed layer temperature and depth remain steady, since the small wind velocity and net cooling are not enough to overcome the thermal and mechanical inertia of the mixed layer. Additionally, the developed current velocities are small, which in turn means that the advective terms are negligible. When the wind starts to blow more strongly, after 24 hours, the mixed layer starts to sink in the regions N and F, with a time lag of 10 hours in N and 4 hours in F. This time lag response must be associated with the initial mixed layer depth h, 100 m at N and 45 m at F. However, in region S with initial mixed layer depth of 60 m, h remains unchanged, indicating that there is another

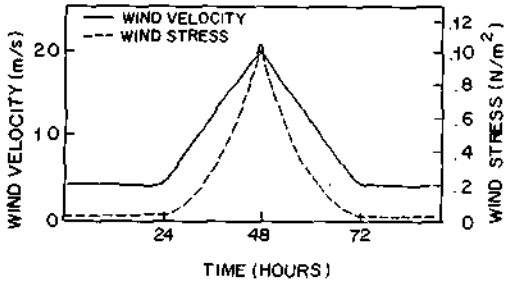

Figure 5. Time variation of the wind velocity, u_a (solid line), and wind stress, $|\tau|$ (dashed line).

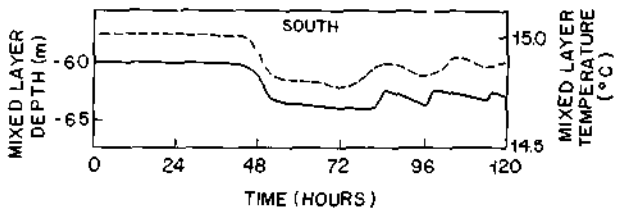

Figure 7. Time variation of mixed layer temperature (dashed line) and mixed layer depth (solid line) in the region south of the front (S).

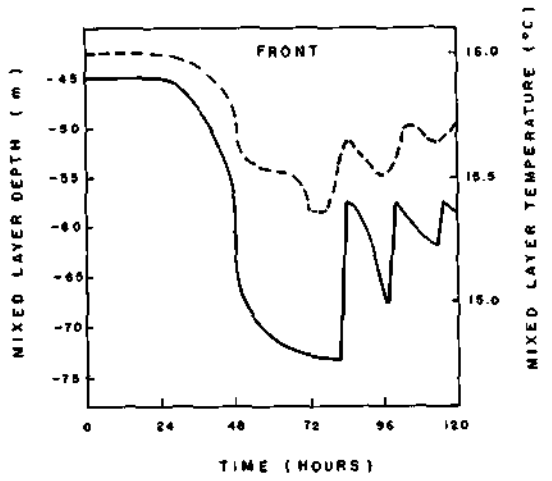

Figure 8. Time variation of mixed layer temperature (dashed line) and mixed layer depth (solid line) in the frontal region (F).

important factor in the temperature and mixed layer depth: the dependence on temperature gradients above the thermocline which are much stronger in region S.

Initially, the sinking and cooling rates are small and reach a sudden maximum around 48 hours. This coincides with the maximum wind intensity. Here we have an indication that the sinking and cooling of the mixed layer is not a smooth process, in accordance with *Elsberry and Camp* [1978]. The maximum depth is reached at approximately 72 hours, reaching 64 m in region S, 73 m in F, and 120 m in N. After this the mixed layer remains steady for about 8 hours, starting to retreat due to weak winds and diurnal heating.

The local inertial period is 18.6 hours (latitude 40°S), and due to the horizontal advection terms, there is an oscillation at around 16 hours. At each quasi-inertial period, there is a retraction of the mixed layer, and the maximum depth is never reached again. The sudden decrease of the mixed layer depth and the delay (2 hours) in starting the retraction (when the maximum depth is reached) are numerical demands made in order to avoid numerical instabilities when the sinking/cooling regime is changed to the retraction/heating regime. Thus this apparent discontinuity is not a real phenomenon. What should be emphasized, nevertheless, is that an oscillation with a frequency a little longer than the local inertial ("shift to the blue") must exist.

The temperature, in turn, continues to decrease until approximately 54 hours when the rate of decrease falls off considerably. Around 60 hours, the rate of temperature decrease is quasi-steady, coinciding with one of the peaks of heat gained by the ocean. The minimum temperature is reached at 72 hours with the values of 14.8°C in S, 15.4°C in F, and 19.4°C in N, constituting a total variation of 0.2°C, 0.6°C, and 0.6°C, respectively. Therefore for a storm that develops symmetrically with respect to time, the maximum depth and the minimum temperature coincide with the return of fair atmospheric conditions. Thereafter, there is no further temperature decrease, with the temperature oscillating with a frequency less than the inertial (shift to the red). At approximately every 20 hours, there is a mixed layer warming, but the temperature never reaches the previous minimum point; also the amplitude of the oscillations displays a decreasing trend.

The difference between the oscillation frequency of temperature and that of the mixed layer depth is due to the difference between the thermal inertia (large) and mechanical inertia (small) of the mixed layer. In addition, the temperature should follow closely the diurnal heating cycle. The phase difference between oscillations of h and T should not reach 180°, since before this happens, the oscillations will be damped. This damping process is more intense when a sharp thermocline exists at the base of the mixed layer.

The comparison of the temperature profiles when the storm begins (24 hours) and ends (72 hours) for the regions S, F, and N (Figure 10) shows, in general, that only the layer just below the mixed layer exhibits a slight increase in temperature, with the deeper layer conditions remaining unchanged. Inside the mixed layer the cooling is due to entrainment and to the surface buoyancy flux. For the layers just below the mixed layer the heating is caused by entrainment. Although this heating could be caused by a convective adjustment of the profiles, (when $R_i^* < 0.25$), it could be inferred that the heating magnitude decreases with the increase of the vertical gradient of temperature in the base of the mixed layer. For the deeper layers the temperature changes must be mainly due to the advective terms, which are small.

A small displacement of the front toward the south is suggested by Figure 11, showing the vertical velocity versus cross-front distance (y coordinate), where the curves for the

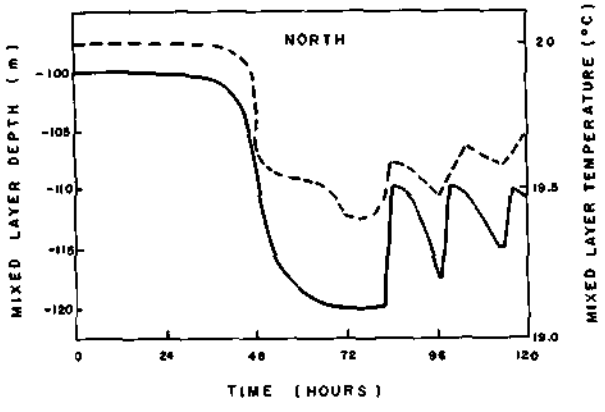

Figure 9. Time variation of the mixed layer temperature (dashed line) and mixed layer depth (solid line) in the region north of the front (N).

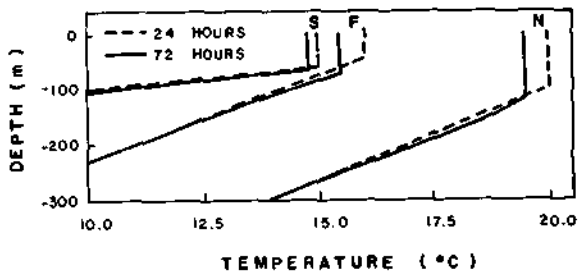

Figure 10. Temperature profiles in the regions south (S) and north (N) of the front and also the temperature profiles in the frontal region (F), when the storm starts (dashed line) and when it ends (solid line).

beginning and the end of the storm are shown. The horizontal divergence field in the mixed layer is expressed in an equivalent manner by the vertical velocity field in the layer just above that which contains the base of the mixed layer. The positive vertical velocities indicate upwelling or horizontal divergence, while the negative ones indicate downwelling or horizontal convergence. When the wind starts to blow there is a slight upwelling (divergence) in the regions S and N associated with the downwelling at F, assuring mass conservation. At the end of the storm event the upwelling and the downwelling are intensified, with the downwelling maximum being shifted approximately 20 km toward the south with respect to the initial maximum. This ocean front shift in response to a single storm event does not agree with *Roden and Paskausky* [1978], who assert that the response time is 1 week.

When comparing the mixed layer depth variations with temperature variations, it would be expected that the variation of the temperature profile at F would be greater than 0.6°C, since there was a 28 m sinking during the total process. This is probably due to the tendency of the downwelling to cause a slight warming of the mixed layer, contrary to the cooling caused by the upwelling.

The anomalous upwelling observed near the boundaries (see Figure 11) is spurious and due to the somewhat inadequate boundary conditions. As the vertical velocity is computed from the continuity equation (equation (3)), where there is a horizontal derivative, the horizontal velocity error at the boundary is amplified. However, for the time step of integration used, these errors do not affect the regions of interest, S, F, and N.

The evolution of the velocity field in the mixed layer and in the layer just under the mixed layer base, for the three regions, S, F and N, is shown in Figure 12. During the first time step the velocities at S and F are larger because the mixed layer depths are shallow. After the sudden wind stress increase (24 hours), the mixed layer modeled velocities also increase suddenly and not in a continuous form, but with peaks separated by roughly regular 20-hour intervals. These oscillations, although persistent in the mixed layer, are not found in the layer below, in agreement with *Halpern* [1974] and disagreement with *Price* [1976]. By the time of the current velocity maximum (70 hours), there is a vertical shear between the velocity in the mixed layer and the velocity at the top of the thermocline of approximately 0.27 m/s in S, 0.20 m/s in F, and 0.15 m/s in N. This strong shear

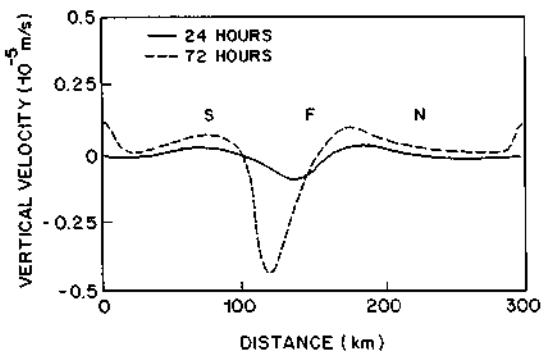

Figure 11. Cross-front vertical velocity when the storm starts (solid line) and when it ends (dashed line).

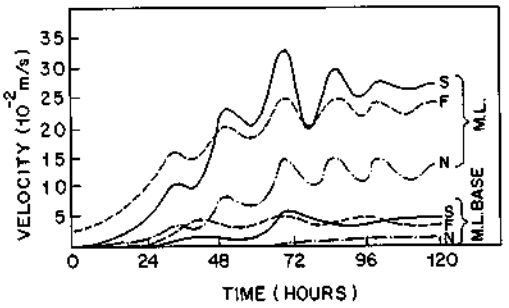

Figure 12. Time variation of the mixed layer current velocity at the regions S (solid line), F (dashed line), and N (dash-dot line). The current just below the mixed layer in these regions is also shown.

results in $R_i^* < 0.25$, confirming the idea that the mixed layer is essentially turbulent. It should be noted, however, that the velocity variation in the layer below the mixed layer is very small, making a small contribution to the intensification of the velocity shear.

The response time before indications of inertial oscillations is about 10 hours. This is small when compared to the inertial period and is due to the small mechanical inertia of the mixed layer.

The intensity of the velocity in the mixed layer during strong wind periods is directly related to the mixed layer depth [*Phillips*, 1977]. With the return to mild wind conditions, the modeled current velocities in the mixed layer show a temporal variability that is dominated by movements with a period of approximately 16 hours. Thus the dominant wave frequency exceeds the inertial by 16% (shift to the blue).

The existence of inertial oscillation suggests the following sequence in the development of the observed (modeled) currents [*Pollard*, 1970; *Pollard and Millard*, 1970; *Phillips*, 1977; *Pollard*, 1980; *D'Asaro*, 1985b]. During the period of intense wind stress, Ekman currents are generated, and when the wind stress slackens, these currents are too weak to be maintained by geostrophic balance because the pressure gradient terms will be small compared to Coriolis. The dominant balance will then be between the inertial terms and Coriolis, and the current will turn inertially. The pressure gradient terms, though comparatively small, have the tendency to restore the geostrophy, being important in the energy dissipation process.

The temporal behavior of the along-front velocity component (u) and cross-front velocity component (v) for the regions S, F, and N is shown in Figures 13, 14, and 15. The u component increases continually and does not oscillate until 72 hours. Thus the nonlinear terms of the x momentum equation are not important while the wind is strong. There is a small-amplitude oscillation which is swiftly damped after the wind decreases. After 10 hours of stronger winds the v component starts to oscillate with large amplitudes, reaching its maximum value approximately at the end of the storm. The v oscillations are the ones that modulate the current velocity oscillations. As mentioned before, in the beginning of the experiment there is a tendency for oscillations to have a period larger than the inertial ones (20 hours). However, after the storm the period of oscillation is less (16 hours). This is due to the fact that in the beginning only the meridional component (v) oscillates with a period close to 20

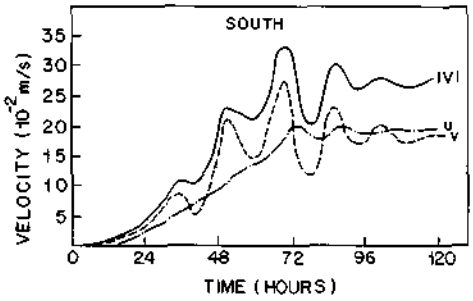

Figure 13. Time variation of the current velocity south of the front (S): its absolute value |v| (solid line); meridional component v (dashed line); and zonal component u (dash-dot line).

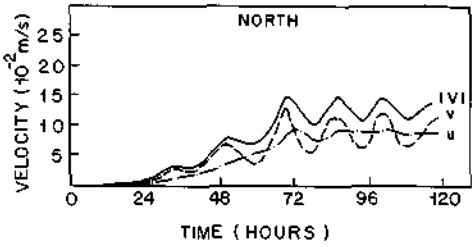

Figure 15. Time variation of the current velocity north of the front (N): its absolute value |v| (solid line); meridional component v (dashed line); and zonal component u (dash-dot line).

hours. After the storm there is an oscillation in u, which, being out of phase with the v component and having different frequencies, results in an oscillation shifted to frequencies higher than the inertial.

The inertial oscillations could be also observed in the velocity diagrams (Figures 16, 17, and 18) for the regions S, F, and N, where the numbers shown indicate the inertial periods (18.6 hours for 40°S). As can be seen, the current increases up to four inertial periods, when it begins to oscillate at inertial frequency, turning around in the anticlockwise sense. The amplitude and damping of this oscillation decrease toward the north, being larger in S and smaller in N. This is probably related to the mixed layer depth at the time when the wind stress becomes negligible.

As final comments on this experiment we can infer that concerning the ocean conditions, two quantities are fundamental in the determination of the delay of response and of the sinking/cooling rate of the mixed layer: the initial mixed layer depth and the intensity of the vertical gradients at the top of the thermocline.

Apparently, the preponderant factor is the thermocline intensity. For instance, in the S region the initial mixed layer depth is 60 m, intermediate between the values of 45 m at F and 100 m at N, but with strong vertical temperature gradients at the base of the mixed layer. In the S region, nevertheless, sensible variations were not detected either in temperature (ΔT = 0.2°C), or in the mixed layer depth (Δh = 4 m). In the N and F regions, where the vertical temperature gradients are not so strong, the response time is small compared to the local inertial period. These facts are justified since the stronger the stratification below the mixed layer, the larger R_i^*, which is directly related to Δb. This will inhibit the entrainment and consequently will retard or hinder the mixed layer sinking/cooling.

During the storm event it was observed that the mixed layer depth could increase and the temperature decrease, even though the ocean is being heated. This is the result of entrainment of cooler and denser water from the layers below the mixed layer. The downward buoyancy flux needed for entrainment is provided by the wind.

Thus the numerical experiment I (EXP.I) shows that the local changes of the thermal structure of the upper ocean are due to the superposition of the entrainment effect and heat lost to the atmosphere through surface fluxes. The relative amount of the contribution of each is studied in EXP.II, discussed in the next section.

4.3. Results and Discussion of EXP.II

In this experiment the surface buoyancy flux is suppressed in order to try to separate its influence in the thermal and dynamical structure of the ocean front from the influence of the buoyancy flux due to entrainment at the base of the mixed layer. The comparisons between EXP.II and EXP.I will be made only for the F region, which characterizes the upper ocean structure in a surface ocean front with respect to the regions S and N. No significant variation could be detected compared to F.

The temporal variation of velocities in the mixed layer and in the layer just below shows absolutely analogous behavior, in spite of the large heat loss ($Q = -27.2 \times 10^6$ W/m^2) which occurred during the 5-day integration period in EXP.I.

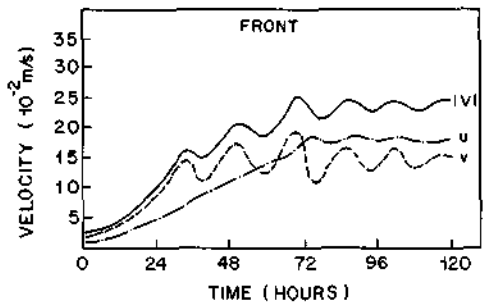

Figure 14. Time variation of the current velocity in the front (F): its absolute value |v| (solid line); meridional component v (dashed line); and zonal component u (dash-dot line).

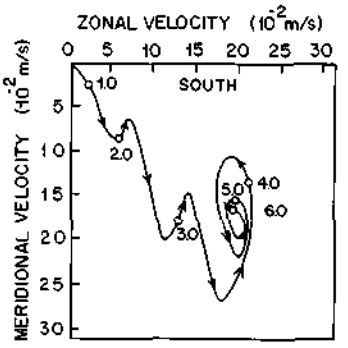

Figure 16. Velocity hodograph in region S. The numbers indicate local inertial periods, and the arrows indicate the direction (the inertial period for 40°S is 18.6 hours).

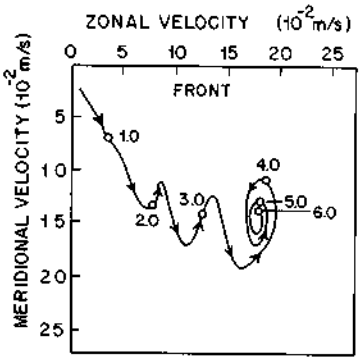

Figure 17. Velocity hodograph in region F. The numbers indicate local inertial periods, and the arrows indicate the direction (the inertial period for 40°S is 18.6 hours).

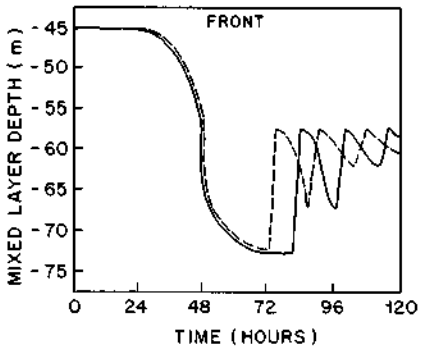

Figure 19. Time variation of mixed layer depth at the front from numerical experiments I (solid line) and II (dashed line).

The comparative evolution of the mixed layer depth is shown in the Figure 19, where we can note a maximum decrease of about 4% of the total depth variability, at 72 hours.

These results show that at least for small timescales and very strong wind conditions considered here, the surface heat exchange is not important in the determination of the mixed layer velocities and depth. Besides that, the entrainment velocity, w_e, is approximately the same, indicating that the kinetic energy generated by shear (mechanics) is more important than the energy generated by temperature differences (convective). The sinking process is really dominated by the wind stress through the term u_*^3. Probably, as asserted by *Kraus and Turner* [1967], the cooling could be more important than the wind stress in the dynamic change of the mixed layer, but only under mild wind conditions or on seasonal timescales, where a climatological wind stress mean is considered.

After 72 hours, there is a stabilization of the mixed layer depth caused by numerical adjustments, followed by a sudden retraction, which is anticipated by 15 hours in the same experiment performed with inclusion of surface heat flux. The minimum mixed layer depth reached during the retraction is the same (57.5 m). Thus the response time for the beginning of the inertial oscillations depends not only on the preexistent water column conditions, but also on the atmospheric conditions at the moment. The mixed layer depth oscillation period was the same for the two experiments (16 hours); this demonstrates the importance of the nonlinear terms in mixed layer models.

The mixed layer temperature suffered more sensible changes in the experiments than the mixed layer depth. Figure 20 shows the temporal behavior of the temperature for the two experiments (EXP.I and EXP.II).

Without the surface buoyancy fluxes the temperature variation is continuous from 24 to 72 hours of simulation. The maximum rate of temperature decrease remains around 48 hours, but in this experiment the temperature does not display steadiness at around 60 hours, suggesting that the temperature variation was due to diurnal heating. The minimum temperatures reached in both experiments were slightly different, showing that under storm conditions, the entrainment is more important in the decreasing temperature process than the surface heat loss. After 72 hours, during the mild wind conditions, there was no oscillation due to the diurnal heating. The temperature decreases slowly and systematically, indicating nonlinearity effects through the nonconstant cooling rate.

The attempt to conserve the amount of heat, imposed by the formulation of the problem, results in an instability in the layers below the mixed layer, which in turn compels many iterations in order to obey the requirement $R_i^* \geq 0.25$. We cannot make any conclusive remark about the behavior of the mixed layer temperature beyond 72 hours because, apparently, some numerical problems arise after that time

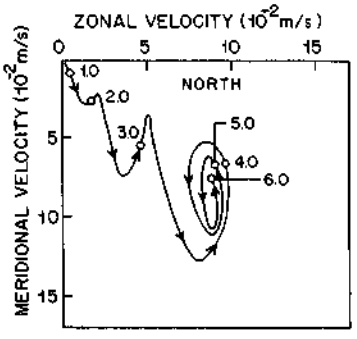

Figure 18. Velocity hodograph in region N. The numbers indicate local inertial periods, and the arrows indicate the direction (the inertial period for 40°S is 18.6 hours).

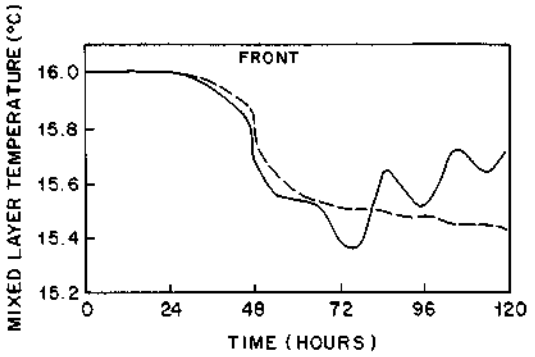

Figure 20. Time variation of mixed temperature at the front from numerical experiments I (solid line) and II (dashed line).

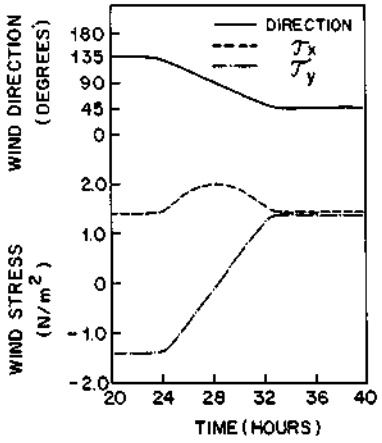

Figure 21. Time variation of the wind direction $\beta(t)$ (solid line), x component of the wind stress (dashed line), and y component of the wind stress (dash-dot line) for experiment III.

due to the Richardson number condition, invalidating the results.

4.4. Results and Discussion of EXP.III

The frontal phase of an atmospheric cold front is characterized by a sudden change in the wind direction, without large changes in its magnitude [*Thompson and Huggett*, 1981]. The purpose of this experiment is to verify in which sense the change in the wind direction could affect the ocean front structure.

The initial fields of temperature, mixed layer depth, and current velocity, as well as the heat exchange processes in the air-sea interface, will be the same as EXP.I. The wind stress, $\tau(t)$, will have its components given by

$$\tau_x(t) = \rho_a C_D u_a^2 \sin \beta(t)$$
$$\tau_y(t) = \rho_a C_D u_a^2 \cos \beta(t) \tag{22}$$

where β is the angle between the north and the direction from which the wind is blowing. The wind speed is constant and equal to 4 m/s during the simulation period. The temporal variation of $\beta(t)$, $\tau_x(t)$, and $\tau_y(t)$ is shown in Figure 21.

The NW wind direction in the first 24 hours is constant; after that there is a change in the direction at a constant rate of 10°/h, reaching the SW direction after 9 hours. In the following hours the wind is constant in magnitude and direction.

As pointed out before, the only purpose of this experiment is to investigate the thermal and dynamical response of a vertical section of a horizontally nonhomogeneous ocean to the change of wind direction only.

The temperature and the mixed layer depth at the region N remained unchanged, probably due to the large depth of the mixed layer and the lack of entrainment at its base. The regions F and S present the same qualitative behavior under the imposed atmospheric forcing, differing only in the order of magnitude of the variations. Since the variations are very small and better visualized at F, the temperature and horizontal velocity graphs will be shown for this region only.

The temperature variation is shown in Figure 22. Due to the low wind speed and small initial warming, the temperature remains unchanged during the first 36 hours. From then on, there is a small temperature decrease with a maximum variation rate around 48 hours. About 55 hours there is an inversion in the rate of decrease, reaching an intermediate maximum about 60 hours. During the remaining period of numerical integration there is an oscillation with the diurnal heating cycle showing no damping. Despite the existence of a strong horizontal temperature gradient in the F region, the advective terms are not important due to the low current velocities developed. Probably in a timescale larger than the one considered here, some kind of oscillation could be generated by those terms. The layers below the mixed layer does not show any variation in temperature, since the vertical advection terms are also negligible. Thus the temperature field does not feel the change in the wind direction, as its variations are due only to the surface buoyancy fluxes.

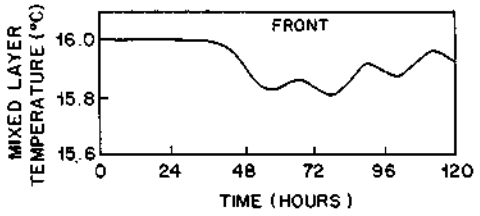

Figure 22. Time variation of the mixed layer temperature, at the frontal region for experiment III.

The mixed layer depth also did not show significant variations. Even if the water column potential energy should be conserved since the low value of u_* does not allow entrainment in the mixed layer base, it is proportional to the square of the mixed layer depth and to the linear temperature. With such small temperature variation, the mixed layer depth remained unaffected.

Figure 23 shows the temporal variation of the mixed layer horizontal velocities. The initial speed is 0.025 m/s, with a larger meridional component (v = 0.023 m/s). There is a small decrease in the beginning as an adjustment of the model to the imposed forcing. Up to 24 hours the current velocity is increasing, but always with small values due to the low wind velocity. Just after the wind direction change there is a change in the rate of increase, even changing to a decreasing rate (around 27 hours) due to the change of sign of the v component, before stabilizing and remaining approximately constant in direction and magnitude for the rest of the time.

The u component exhibits similar behavior up to 24 hours,

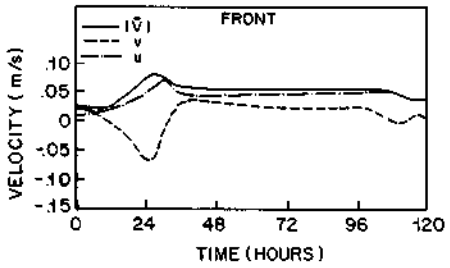

Figure 23. Time variation of the current velocity (solid line), meridional component v (dashed line), and zonal component u (dash-dot line) at the frontal region for experiment III.

with a slightly higher rate of increase in the velocity after that, due to the intensification of the x component of the wind stress. After that, there is a decrease with a tendency to reach a constant value, never changing sign, but with a slight increase with time.

The v component decreases continuously, reaching its minimum value at 24 hours, when it starts to increase at a higher rate due to the variation of the external forcing. The maximum value is attained around 36 hours, with an absolute value much less than that attained at 24 hours. After that, there is a slow damping, probably due to the diffusive terms.

The observed oscillations after 90 hours of numerical integration are spurious and due to the boundary conditions. Despite special treatment of the pressure gradient term and the boundary conditions, in this model, a sudden perturbation in the system makes unavoidable some boundary reflections.

Taking into account only the external factors, the sinking process and the maximum current attained in the mixed layer are uniquely dependent on the intensity of the applied wind stress. Although in this case the advective terms did not exert any significant influence in the maintenance and propagation of the oscillations in the mixed layer, it could be noticed that a sudden change in the wind direction induces perturbations in the mixed layer more quickly than a constant strong wind acting during many hours. Therefore for forecasting at this timescale, the wind climatological means for the region are not appropriate, since the response time is swift and very sensitive to the local wind variation.

The spatial variation of the vertical velocity along the front before and after the wind direction change is shown in Figure 24. Here we can observe that in spite of the small values of the velocity, there is an almost complete inversion of upwelling and downwelling processes and vice versa.

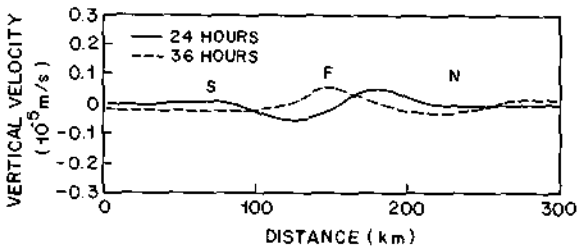

Figure 24. Vertical velocity field in a cross-front section, at the beginning of the wind direction change (solid line), and at the end of the wind direction change (dashed line).

5. Conclusions

5.1. Critical Analysis of Model Limitations

Before summarizing the main conclusions, is perhaps appropriate to mention the principal limitations involved in the analysis. The errors in the prediction of the thermal and dynamical structures of the upper ocean could be divided into four categories: (1) errors due to uncertainties in the atmospheric forcing computations; (2) errors due to ill-posed initial conditions; (3) errors due to the physical limitations of the model, i.e., its approximations and simplifying assumptions; and (4) errors due to inaccuracy of the numerical solutions.

In the first category, a typical procedure to specify the surface heat and momentum fluxes is through the use of the bulk aerodynamical formulas, which include meteorological surface observations and empirical turbulent coefficients. There are many specific studies of quantitative evaluation of the surface parameters in the computation of atmospheric forcing through the bulk aerodynamic formulas [*Friehe and Schmitt*, 1976; *Fissel et al.*, 1977; *Foken*, 1984; *Stravisi and Crisciani*, 1986]. A brief summary of the main conclusions will be repeated here.

1. The wind velocity is very important because of its triple effect in the dynamics of the upper ocean. First, it induces surface currents. Second, it induces changes in the mixed layer depth through the turbulent kinetic energy that is proportional to u_*^3. Third, it controls the latent and sensible heat transfer between the atmosphere and ocean.

2. The dew point temperature is important, since it is needed in the computation of the latent heat flux, one of the main terms in the budget.

3. The sea surface temperature is important also, since it appears to the fourth power in the computation of the infrared radiation from the sea.

4. The air temperature near the surface and the cloud cover estimates are not as important as the other parameters, since they are linear terms in the computation of sensible heat flux, heating by solar radiation, and cooling by long-wave emission.

5. The selection of values for the bulk transfer coefficients depends on the specific conditions for which the model is proposed. Facing this empirical scenario, one finds a wide range of values in the literature [*Hidy*, 1972]. For instance, in this work we have used *Garratt*'s [1977] drag coefficient (equation (20)), which does not take into account the atmospheric stratification.

Therefore the uncertainty in the wind stress estimates is the largest source of error in the prediction models for the thermal and dynamical behavior of the upper ocean, particularly when we deal with extreme conditions, as in our case.

In the second category, the specific studies on the influence of the initial conditions in the predictive models, through data assimilation techniques [*Elsberry and Warrenfeltz*, 1982], are not yet conclusive. The scope of this study was not to evaluate the effect of different initial temperature and velocity profiles on the mixed layer time evolution. In the mixed layer model of *Martin* [1982], which studied the ocean response to Hurricane Eloise, despite some uncertainties in the initial conditions, the results were reasonably similar.

In the third category, the assumptions and approximations used in the model were justified in section 2. This model is idealized, particularly with respect to the omission of salinity effects [*Miller*, 1976], which does not allow us to consider other characteristic aspects of the passage of atmospheric fronts such as precipitation.

In this model the constant coefficient turbulent diffusivity is a poor parametrization of the horizontal mixing effect in a strongly nonhomogeneous field.

Although the entrainment process was made possible through the ad hoc parametrization of the "buoyancy" flux at the base of the mixed layer, this parametrization does not have any incontestable experimental support. The sensitivity of the results for different parametrizations of the entrain-

ment, horizontal mixing, and dissipation processes could be the subject of further studies.

When some dynamic parameter reaches a typical value, instabilities could occur. The mixed layer models utilize the Richardson gradient number (R_i), which relates thermodynamical (density differences) to dynamical (vertical shear velocity) quantities. However, it is inherently vulnerable to the choice of the distances over which the jumps in the variables are estimated. It is the judgment of these distances that will cause the critical values to be reached or not; this leads us to a critical point, which is based on a not very rigorous criterion, in provoking or not provoking instabilities in the water column.

In the fourth category the numerical schemes used in this model are expected to guarantee numerical stability under all circumstances during the integration time (120 hours). Nevertheless, around the time step number 90 (45 hours of integration), the term ∇P starts to become very large near the boundaries. This would lead to large differential velocities, which have a tendency to destabilize the vertical velocity computation, estimated through the continuity equation. Probably, this is due to the instability of the numerical schemes used to implement the radiational boundary condition, or to the incorrect estimate of the phase velocity of propagation. In order to avoid problems in the region between the tenth and fiftieth grid point, an artificial damping was imposed for the points outside of this region, by the use of diffusion coefficients 2 orders of magnitude larger, after the fiftieth time step.

If a larger numerical integration time is needed, for instance, to evaluate the time needed to have the inertial oscillations completely attenuated after the storm in EXP.I, these boundary conditions must be recalculated.

Models of prediction for the upper ocean are initial boundary value problems, which are very much dependent on meteorological and oceanographical observations. Up to the present, the lack of an adequate data set for numerical simulations is the largest obstacle for the general development of the numerical prediction models, such as the one here presented.

5.2. Summary of the Main Conclusions

The results obtained and discussed in section 4 have shown that this model can be used to estimate the magnitude of the thermal and dynamic changes of the upper ocean. Also the response time of those changes to a sudden intensification in the momentum and heat fluxes in the air-sea interface can be estimated. The principal conclusions of this study can be summarized as follows:

1. Generally speaking, there were significant increases in the mixed layer depth and decreases in its temperature with the intensification of the wind velocity and surface cooling. Under mild wind conditions and surface heating, there was a retraction of the mixed layer with an associated increase in its temperature.

2. The sinking/cooling process of the mixed layer was not smooth, having its maximum rate coincident with the maximum storm conditions. For a storm symmetrical in time, the maximum mixed layer depth and minimum temperature coincide with the return to the mild atmospheric conditions, since from then on there were no additional sinking or temperature decreases. However, we observed oscillations with frequency near the local inertial frequency in the mixed layer depth (shifted toward blue) and in the temperature (shifted toward red). The phase shifts in h and T are due to differences in the thermal and mechanical inertia of mixed layer and to the diurnal heating cycle and should not reach 180°. The damping process of the oscillations is more intense when there is a sharp vertical gradient of temperature at the base of the mixed layer.

3. In decreasing order of importance, the distributions of momentum and heat in the mixed layer depend mainly on the thermocline intensity at the mixed layer base, wind stress intensity, and mixed layer depth. The entrainment at the mixed layer base, the vertical advection, and the air-sea heat exchange contribute to the sinking/cooling process of the mixed layer. For very short timescales, and under severe wind conditions, the turbulent mixing is basically controlled by u_*^3, favoring entrainment over surface heat exchange. On the other hand, heat losses weaken the stratification; consequently, the resistance to the mixing is also weakened. Thus it is clear that when both processes are combined, as during a cold front passage, the result is maximized.

4. The present model suggests that the ocean response, in terms of mixed layer sinking, to swift and intense atmospheric forcing is also fast, being of the order of 10 hours. It suggests also that thermocline intensity is important in this response time, as well as in the response amplitude.

5. The increases in the wind velocities have a pronounced influence in the mixed layer velocity. The storm excited inertial currents (of the order of 0.3 m/s), whose magnitude depends on the mixed layer depth. After the storm passage, this inertial current rotates in the anticlockwise direction and decreases in magnitude. The oscillation frequency is larger than the local inertial frequency by 16% (blue shift), with the respective damping directly related to the mixed layer depth at the moment that the wind stress becomes negligible. The current velocity components u and v are out of phase and have different oscillation frequencies.

6. The inertial oscillations do not propagate in the layers below the mixed layer depth, and their thermal and dynamical structures were not modified.

7. Usually, the advective timescale is larger than the synoptic timescale we deal with in this problem. However, through horizontal inhomogeneities and atmosphere-ocean heat fluxes the advective terms become important as they result in inertial oscillations of mixed layer properties once mild atmospheric conditions are reestablished. This is one of the aspects that show the need to have the mesoscale dynamics associated with the mixed layer dynamics for short-term prediction in the ocean. Nevertheless, for small wind velocities, the inertial terms are negligible, which suggests a decoupling of the level model and the mixed layer model. Thus the studies of the thermal and dynamic changes in the upper ocean, even in an ocean front, could be done using unidimensional mixed layer models, but only over a seasonal timescale.

8. The development of a storm over an existing ocean front was able to displace the front from its initial position by approximately 20 km. It should be noted that the displacement of a strong baroclinic zone such as the subtropical convergence in the South Atlantic, could bring important consequences to the atmosphere. For instance, *Sanders and Gyakum* [1980] found a large correlation between marine cyclogenesis events and strong sea surface temperature gradients.

9. The thermal structure of the upper ocean, in this experiment, is totally indifferent to a change in wind direction, for low-intensity winds, even in regions where there are strong horizontal gradients, as in an ocean front. The oscillations of the mixed layer temperature are entirely a function of the daily scale of the solar heating.

10. For a sudden change in the wind direction, the response of the current velocity field in the mixed layer is almost instantaneous.

5.3. Suggestions

This work was dedicated to understanding how a solitary atmospheric event contributes to the variability of a large-scale ocean front. Since the response timescale of the ocean is much larger than the atmospheric forcing timescales, this would justify the use of the temporal mean of the forcing in ocean simulations. However, under severe atmospheric conditions, significant changes do occur in the ocean thermal structure on short timescales. Even using an idealized characterization of one of the phases of an atmospheric cold front, these changes are very complex, according to the model.

From the fact that the momentum and heat fluxes at the air-sea interface with respect to the atmospheric cold front passage are very asymmetric and that the thermal and dynamical structure differs from place to place, we can conclude that the ocean response could not easily be generalized. Thus the presented results should be interpreted with caution, since the precise description of the fast ocean response to storms can only be reached by the means of many events. In addition, during each of these events, detailed specification of the atmospheric forcing and of the upper layer structure of the ocean must be given.

Perhaps the least understood aspect of the dynamics of the upper ocean is the horizontal variability of the upper mixed layer. In this model of an ocean front under the action of an atmospheric front, many physical processes were not included. It is premature therefore to compare quantitatively the presented results with real ocean observations. Before these comparisons could be established, other improvements should be incorporated in the model, such as introduction of salinity in the buoyancy fluxes; more realistic current velocity profiles, specifically Brazil and Malvinas current velocities; and other features proposed in section 5.1. Finally, a giant step will be taken with the inclusion of the third dimension in the model.

Acknowledgments. The authors wish to thank Antonio Divino Moura for helpful comments and enlightening discussions during the progress of the work and Mark Cane and Andre Visser for their comments and criticisms on an earlier draft. Araceli Melendez Crosthwaite is thanked for typing the manuscript and Gilberto Fuentes and Ramon Moreno C. for producing the drawings. Critical comments by the reviewers helped to improve the manuscript and are greatly appreciated.

References

Adamec, D., and R. W. Garwood Jr., The simulated response of an upper-ocean density front to local atmospheric forcing, *J. Geophys. Res.*, *90*(C1), 917–928, 1985.

Adamec, D., B. L. Elsberry, R. W. Garwood Jr., and R. L. Haney, An embedded mixed layer ocean circulation model, *Dyn. Atmos. Oceans*, *6*(1), 69–96, 1981.

Camerlengo, A. L., and J. J. O'Brien, Open boundary conditions in rotating fluids, *J. Comput. Phys.*, *35*(1), 12–35, 1980.

D'Asaro, E. A., Upper ocean temperature structure, inertial currents, and Richardson numbers observed during strong meteorological forcing, *J. Phys. Oceanogr.*, *15*(7), 943–962, 1985a.

D'Asaro, E. A., The energy flux from the wind to near-inertial motions in the surface mixed layer, *J. Phys. Oceanogr.*, *15*(8), 1043–1059, 1985b.

Dillon, T. M., and D. R. Caldwell, Catastrophic events in a surface mixed layer, *Nature*, *276*(5688), 601–602, 1978.

Elsberry, R. L., and N. T. Camp, Oceanic thermal response to strong atmospheric forcing, I, Characteristics of forcing events, *J. Phys. Oceanogr.*, *8*(2), 206–214, 1978.

Elsberry, R. L., and S. D. Haney, Sea-surface temperature response to variations in atmospheric wind forcing, *J. Phys. Oceanogr.*, *8*(5), 881–887, 1978.

Elsberry, R. L., and L. L. Warrenfeltz, Data assimilation test with an oceanic mixed layer model, *J. Phys. Oceanogr.*, *12*(8), 839–850, 1982.

Elsberry, R. L., S. A. Sandgathe, and F. J. Winninghoff, Short-term oceanic response predicted by a mixed layer model forced with a sector atmospheric model, *J. Phys. Oceanogr.*, *14*(1), 79–91, 1984.

Fissel, D. B., Spectral analysis of surface atmospheric quantities at ocean weather-ship P, *Atmosphere*, *14*(2), 77–97, 1976.

Fissel, D. B., S. Pond, and M. Miyake, Computation of surface fluxes from climatological and synoptic data, *Mon. Weather Rev.*, *105*(1), 26–36, 1977.

Foken, T., The parameterization of the energy exchange across the air-sea interface, *Dyn. Atmos. Oceans*, *8*(3), 297–305, 1984.

Frankignoul, C., Sea surface temperature anomalies, planetary waves, and air-sea feedback in the middle latitudes, *Rev. Geophys.*, *23*(4), 357–390, 1985.

Friehe, C. A., and K. F. Schmitt, Parameterization of air-sea interface fluxes of sensible heat and moisture by the bulk aerodynamic formulas, *J. Phys. Oceanogr.*, *6*(6), 801–809, 1976.

Garratt, J. R., Review of drag coefficients over oceans and continents, *Mon. Weather Rev.*, *105*(7), 915–929, 1977.

Garwood, R., Jr., An oceanic mixed layer model capable of simulating cyclic states, *J. Phys. Oceanogr.*, *7*(3), 455–468, 1977.

Girardi, L. C., Análises sinóticas de ciclones extratopicais, *Relatorio Tec.*, *IAE-001*, Inst. de Atividades Espaciais, São José dos Campos, Brazil, 1972.

Godoi, S. S., Estudos das variacoes sazonais da frente oceanica subtropical entre a Corrente do Brasil e a Corrente das Malvinas, utilizando dados oceanográficos e dos satélites SMS-2, Dissertacao de Mestrado em Sensoriamento Remoto, *INPE-2780-TDL/137*, Inst. de Pesqui. Espaciais, São José dos Campos, Brazil, 1983.

Halpern, D., Observations of the deepening of the wind-mixed layer in the northeast Pacific Ocean, *J. Phys. Oceanogr.*, *4*(4), 454–466, 1974.

Haltiner, G. J., and R. T. Williams, *Numerical Prediction and Dynamic Meteorology*, 2nd ed., 477 pp., John Wiley, New York, 1980.

Haney, R. L., A numerical study of the response of an idealized ocean to large-scale surface heat and momentum flux, *J. Phys. Oceanogr.*, *4*(2), 145–167, 1974.

Haney, R. L., M. S. Risch, and G. C. Heise, Wind forcing due to synoptic storm activity over the North Pacific Ocean, *Atmos. Ocean*, *19*(2), 128–147, 1981.

Hidy, G. M., A view of recent air-sea interaction research, *Bull. Am. Meteorol. Soc.*, *53*(11), 1083–1102, 1972.

Ikeda, Y., A. S. Mascarenhas Jr., P. L. Cacciari, and L. V. Nonato, Um levantamento sinótico das convergencias Antartica e Subtropical, *An. Acad. Bras. Cienc.*, *58*, suppl., 111–116, 1986.

Kousky, V. E., Frontal influences on northeast Brazil, *INPE-1269-PE/137*, Inst. de Pesqui. Espaciais, São José dos Campos, Brazil, 1978.

Kraus, E. B., and J. S. Turner, A one-dimensional model of the seasonal thermocline, II, The general theory and its consequences, *Tellus*, *19*(1), 98–106, 1967.

Kullenberg, G. E. B., On vertical mixing and the energy transfer from the wind to the water, *Tellus*, *28*(2), 159–165, 1976.

Legeckis, R. V., and A. L. Gordon, Satellite observation of the

Brazil and Falkland currents—1974 to 1976 and 1978, *Deep Sea Res.*, *29*(3), 375–401, 1982.
Marchuk, G. I., V. P. Kochergin, V. I. Klimok, and V. A. Sukhorukov, On the dynamics of the ocean surface mixed layer, *J. Phys. Oceanogr.*, *7*(6), 865–875, 1977.
Martin, P. I., Mixed-layer simulation of buoy observations taken during hurricane Eloise, *J. Geophys. Res.*, *87*(C1), 409–421, 1982.
Mesinger, F., and A. Arakawa, Numerical methods used in atmospheric models, *GARP Publ. Ser.*, *17*, 64 pp., 1976.
Miller, J. R., The salinity effect in a mixed layer ocean model, *J. Phys. Oceanogr.*, *6*(1), 29–35, 1976.
Nowlin, W. D., and C. A. Parker, Effects of cold-air outbreak on shelf waters of the Gulf of Mexico, *J. Phys. Oceanogr.*, *4*(4), 467–486, 1974.
Orlanski, I., and L. J. Polinsky, On response to mesoscale atmospheric forcing, *Tellus, Ser. A*, *35*(4), 296–323, 1983.
Phillips, O. M., *The Dynamics of the Upper Ocean*, 2nd ed., 344 pp., Cambridge University Press, New York, 1977.
Pollard, R. T., On the generation by winds of inertial waves in the ocean, *Deep Sea Res.*, *17*(4), 795–812, 1970.
Pollard, R. T., Observations and models of the structure of the upper ocean, in *Modelling and Prediction of the Upper Layers of the Ocean*, edited by B. Krause, pp. 102–117, Pergamon, New York, 1977.
Pollard, R. T., Properties of near-surface inertial oscillations, *J. Phys. Oceanogr.*, *10*(3), 385–398, 1980.
Pollard, R. T., and R. C. Millard, Comparison between observed and simulated wind-generated inertial oscillations, *Deep Sea Res.*, *17*(4), 813–821, 1970.
Pollard, R. T., P. B. Rhines, and R. O. R. Y. Thompson, The deepening of the wind-mixed layer, *Geophys. Fluid Dyn.*, *3*, 381–404, 1973.
Price, J. F., Several aspects of the response of shelf waters to a cold front passage, *Mem. Soc. R. Sci. Liege*, *10*, 201–208, 1976.
Price, J. F., Upper ocean response to a hurricane, *J. Phys. Oceanogr.*, *11*(2), 152–175, 1981.
Ramming, H. G., and Z. Kowalik, *Numerical Modelling of Marine Hydrodynamics*, *Elsevier Oceanogr. Ser.*, 368 pp., Elsevier, New York, 1980.
Reid, J. L., W. D. Nowlin Jr., and W. C. Patzert, On the characteristics and circulation of the southwestern Atlantic Ocean, *J. Phys. Oceanogr.*, *7*(1), 62–91, 1977.
Roden, G. I., Thermohaline fronts and baroclinic flow in the Argentine Basin during the austral spring of 1984, *J. Geophys. Res.*, *91*(C4), 5075–5093, 1986.
Roden, G. I., and D. F. Paskausky, Estimation of rates of frontogenesis and frontolysis in the North Pacific Ocean using satellite and surface meteorological data from January 1977, *J. Geophys. Res.*, *83*(C9), 4545–4550, 1978.
Rooth, C. G., and H. D. Ostlund, Penetration of tritium into the Atlantic thermocline, *Deep Sea Res.*, *19*(7), 481–492, 1972.
Sanders, F., and J. R. Gyakum, Synoptic-dynamic climatology of the "bomb," *Mon. Weather Rev.*, *108*(10), 1589–1606, 1980.
Sethuraman, S., A. J. Riordan, T. Holt, M. Stuner, and J. Hinman, Observations of the marine boundary layer thermal structure over the Gulf Stream during a cold air outbreak, *J. Clim. Appl. Meteorol.*, *25*(1), 14–21, 1986.
Stevenson, J. W., Response of the surface mixed layer to quasi-geostrophic oceanic motions, Ph.D. thesis, Div. of Appl. Sci., Harvard Univ., Cambridge, Mass., 1980.
Stravisi, F., and F. Crisciani, Estimation of surface heat and buoyancy fluxes in the Gulf of Trieste by means of bulk formulas, *Boll. Oceanol. Teor. Appl.*, *4*(1), 55–61, 1986.
Thompson, R. E., and W. S. Huggett, Wind driven inertial oscillations of large spatial coherence, *Atmos. Ocean*, *19*(4), 281–306, 1981.
Tokioka, T., Some considerations on vertical differencing, *J. Meteorol. Soc. Jpn.*, *56*(2), 98–111, 1978.
Tseng, Y. C., Estudo do extremo oeste da convergência subtropical do Oceano Atlântico Sul usando imagens do satélite NIMBUS V e dados oceanográficos no período de 1972 a 1973, *Relatorio Tec. INPE-940-TPT/038*, 60 pp., Inst. de Pesqui. Espaciais, São José dos Campos, Brazil, 1976.
Turner, J. S., *Buoyancy Effects in Fluids*, 368 pp., Cambridge University Press, New York, 1973.
Van Woert, M., The subtropical front: Satellite observations during FRONTS 80, *J. Geophys. Res.*, *87*(C12), 9523–9536, 1982.
Veronis, G., Partition of energy between geostrophic and non-geostrophic oceanic motions, *Deep Sea Res.*, *3*, 157–177, 1956.
Veronis, G., *The Role of Models in Tracer Studies: Numerical Models for Ocean Circulation*, 364 pp., National Academy of Sciences, Washington, D. C., 1975.
Welander, P., Wind action on a shallow sea: Some generalizations of Ekman's theory, *Tellus*, *9*(1), 45–52, 1957.

A. da S. Mascarenhas Jr, Universidad Autónoma de Baja California, Instituto De Investigaciones Oceanológicas, Apartado Postal 453, Carretera Tijuana-Ensenada, km. 106, Ensenada, Baja California, C. P., 22830, Mexico.

C. S. Pereira, CPETEC, Instituto de Pesquisas Espaciais, P.O. Box 515, São Jose dos Campas, São Paulo, 12227 Brazil.

(Received November 25, 1991; revised March 28, 1994; accepted March 31, 1994.)